**SPARC-BD-05 /01**
**May 2005**

# RF COMPRESSOR OPTIMIZATION STUDY FOR SPARCII/SPARXINO

C. Ronsivalle *(ENEA/FIS)*, M. Ferrario, B. Spataro (*INFN-LNF*), L. Serafini *(INFN-Milan)*

**Abstract**

For the second phase of the SPARC Project it is foreseen to perform optimized velocity bunching studies in order to provide definitive tests of the usefulness of this bunch compression technique. At this aim the first SPARC accelerating structure will operate in the RF compressor configuration with a short SW 11424 MHz section placed before.
A systematic study based on PARMELA simulations has been done in order to optimize the parameters that influence the compression also in view of the application of this system as injector of the so called SPARXINO 3-5 nm FEL test facility.
Some working points in different compression regimes suitable for FEL experiments have been selected. The stability of these points and their sensitivity to various types of random errors are discussed.

# 1 INTRODUCTION

The second phase of the SPARC Project foresees the use of the SPARC photoinjector [1] to test RF compression techniques aimed to the generation of electron beams with high peak brightness.
The SPARC photoinjector, now under construction in Frascati, consists of a 1.6 cell RF gun operated at S-band with a peak field on the cathode of 120 MV/m and an incorporated metallic photo-cathode followed by an emittance compensating solenoid and three accelerating sections of the SLAC type (2856 MHz travelling wave), the first one embedded in a solenoid composed by an array of 13 coils.
It is devoted to provide a 155 MeV-100 A bunch with a projected emittance less than 2 μm and a slice emittance less than 1 μm for the 50% of slices driving a saturating SASE 500 nm FEL without the use of a compressor scheme.
For the RF compression tests it is planned to use the first SPARC accelerating section as RF compressor, to add a solenoid on the sections #2 and #3 and to place a 11424 MHz (the 4th harmonic of the operating frequency of the TW sections) short linac before the first accelerating structure (fig.1). Figure 2a shows the prototype for the 11424 MHz section consisting of a standing wave 9-cells π-mode linac [2] manufactured and tested in the RF laboratory. The relative electric field distribution computed by SUPERFISH has been used in beam dynamics calculation (fig. 2b).

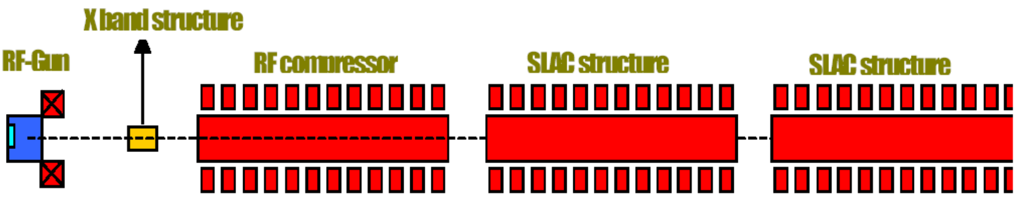


*Fig.1 Sketch of SPARC-phase II layout*

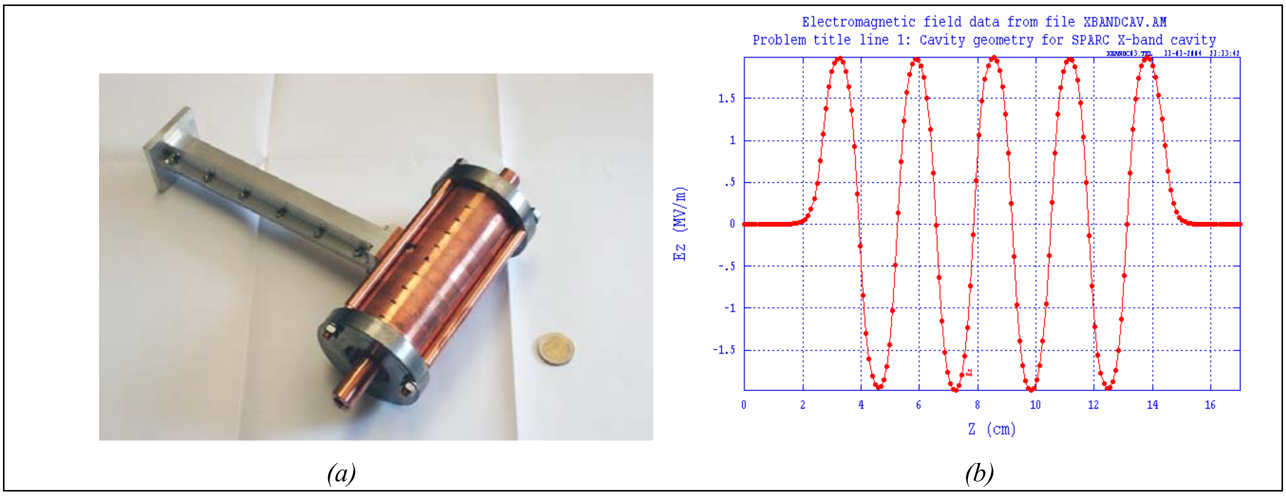


*Fig.2:a) Prototype of the SW X-band linac, b) Electric field distribution on the axis computed by SUPERFISH*

This note presents the results of a systematic study based on PARMELA simulations aimed to optimize the parameters that influence the compression and to investigate the stability and the sensitivity to errors of some useful working points suitable for FEL experiments also in view of the application of the system as injector of the so called SPARXINO 3-5 nm FEL test facility [3].

## 2 RF COMPRESSOR OPTIMIZATION

RF compressor techniques, based on the simultaneous action of velocity bunching and emittance compensation have been theoretically and numerically studied [4,5] and partially confirmed by experimental results [6,7]. In the framework of the second phase of the SPARC Project optimized velocity bunching studies will be performed to provide definitive tests of this technique.
A systematic study based on extensive numerical simulations of beam dynamics with and without the use of a 4th harmonic section placed between the gun and the first TW accelerating section has been done by PARMELA code [8] in order to optimize all the parameters and to study the stability of the system.

### *2.1 No IV harmonic section included*

A first set of PARMELA runs was done to determine the dependence of the final current from the phase on RF compressor and to optimize the magnetic fields in the solenoids embedding the accelerating sections in order to minimize the emittance in different compression regimes without the use of the X-band section. In the calculations the electric field amplitude in the three TW sections was respectively 25,25,15 MV/m.

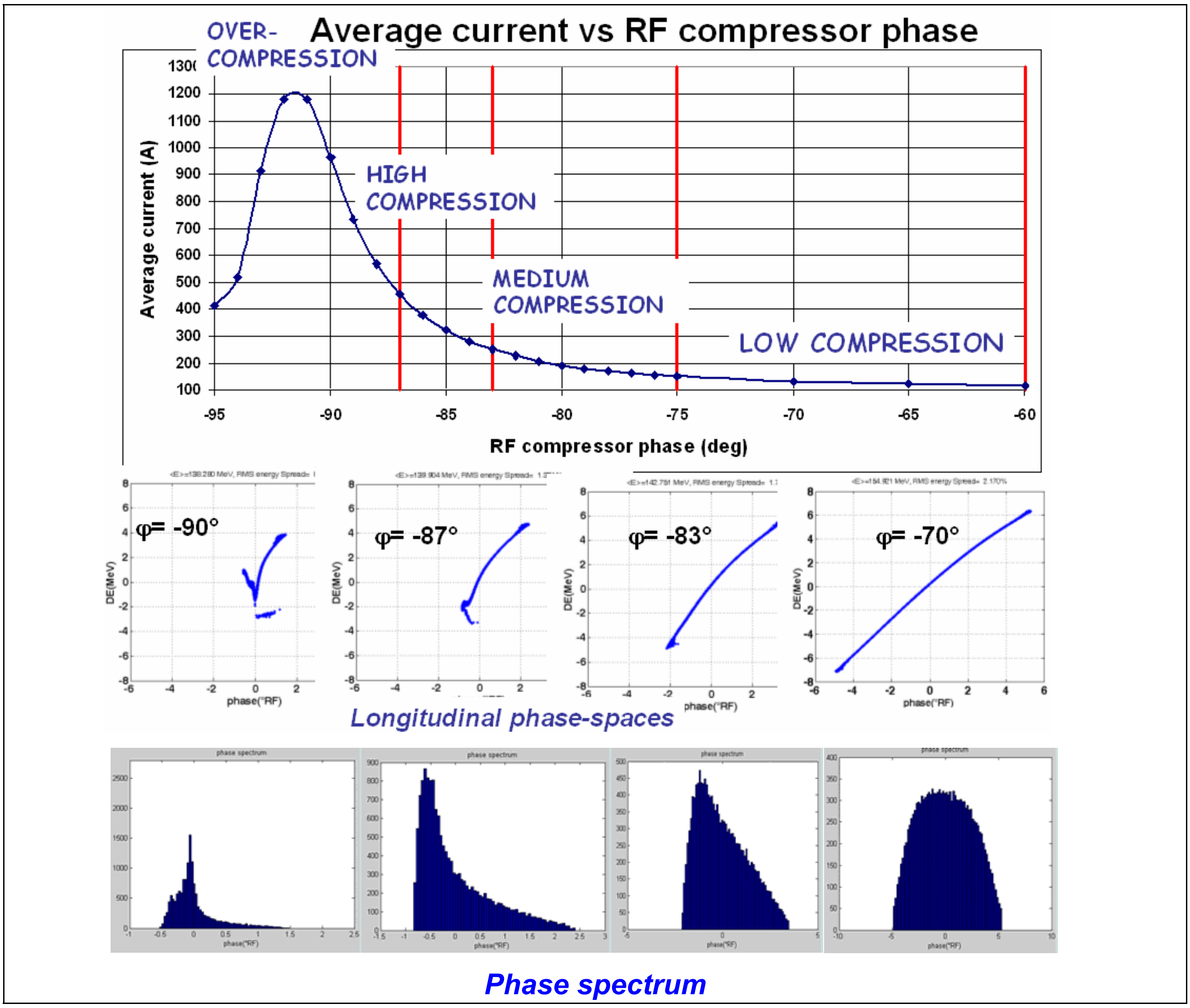


*Fig.3 Dependence from the RF compressor phase of average current, longitudinal phase space and beam phase spectrum*

As it is shown in figure 3 different regimes of compression can be identified each one characterized by different sensitivity to RF compressor phase, different curvature of the longitudinal phase-space and shape of the phase spectrum.
Concerning the RMS energy spread the correlation position-energy required by the bunching process produces a RF chirp that gives an energy spread that decreases with the bunch length, but remains always larger respect to the non compressed beam (fig. 4)

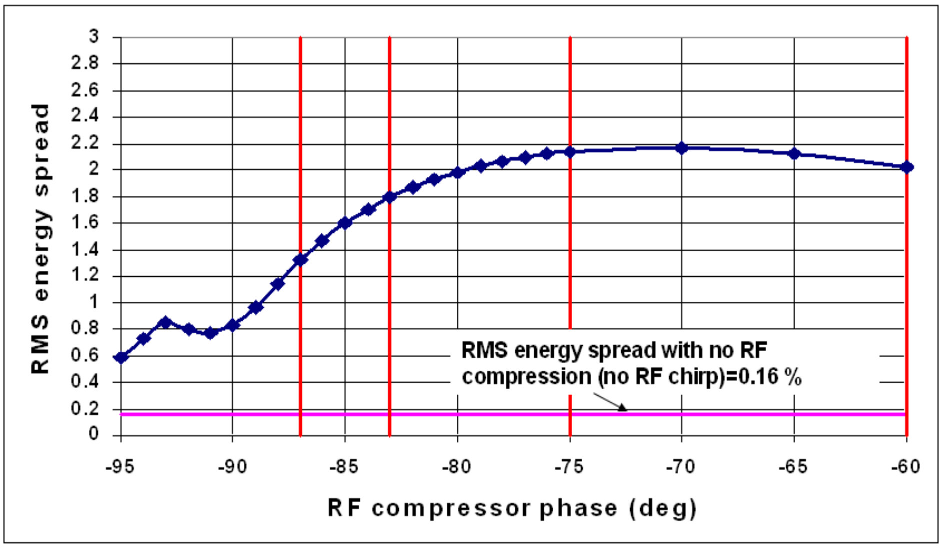


*Fig.4 RMS energy spread vs RF compressor phase*

### *2.1.1 Low compression region (from 117A-165 MeV to 151 A-150 MeV)*

This region, corresponding to a range of RF compressor phase between -60° and -75°, is characterized by a very low distorsion of longitudinal phase space and phase spectrum and low sensitivity to phase jitter (maximum $\Delta I/\Delta\varphi \sim 4$ A/deg).
In the two plots of figure 5 the SPARC non compressed beam is compared with a 151 A beam obtained working with a phase of -75° on the first TW section: it is sufficient to rise the magnetic field on the first section from 615 gauss to 1200 gauss in order to get the same value of final emittance (fig.5a) . The only difference is given by the fact that the RF compressed beam is chirped as it can be observed in figure 5b that shows an increase of RMS energy spread from 0.16% to 2.14%.
This regime of compression, that requires the use of only one solenoid, can be tested just in the phase I of the SPARC Project.

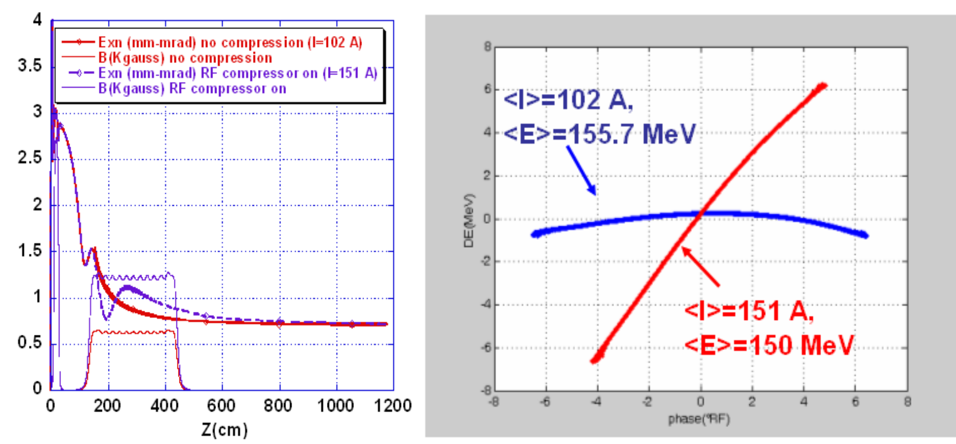


*(a)* *(b)*

*Fig.5 Comparison between the SPARC nominal beam and a 151 A compressed beam: (a) emittance behaviour (b) longitudinal phase space*

### *2.1.2 Medium compression region (up to 249 A-143 MeV)*

In this region, corresponding to a range of RF compressor phase between -75° and -83°, the bunch shape tends to a triangular shape (fig.6) and the sensitivity to phase jitter increases up to $\Delta I/\Delta\varphi$~23A/deg.

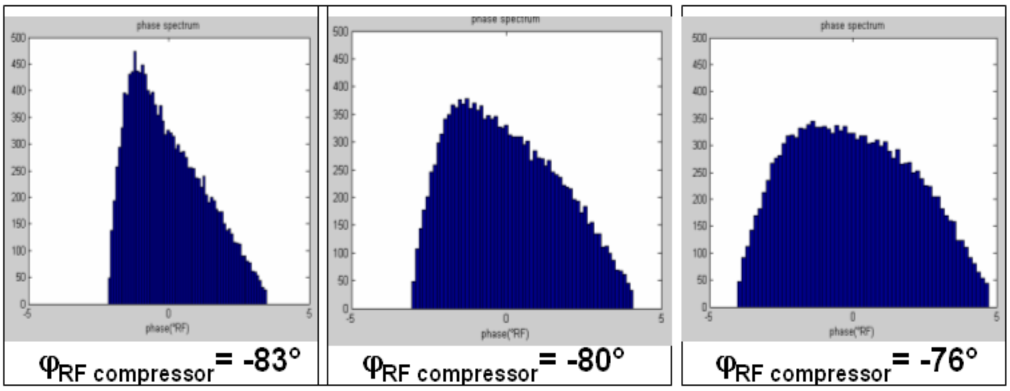


*Fig.6 Evolution of the bunch shape with RF compressor phase in the medium compression region*

Figure 7 shows the case with $\varphi_{RF\ comp}$= -83° corresponding to a current of 249 A: the two plots compare the emittance behaviour if one uses one (B1=1200 gauss) or two solenoids (B1=1200 gauss, B2=1400 gauss). The use of two solenoids allows a better control of envelope and emittance decreasing the value of the final emittance from 1 mm-mrad to 0.8 mm-mrad.

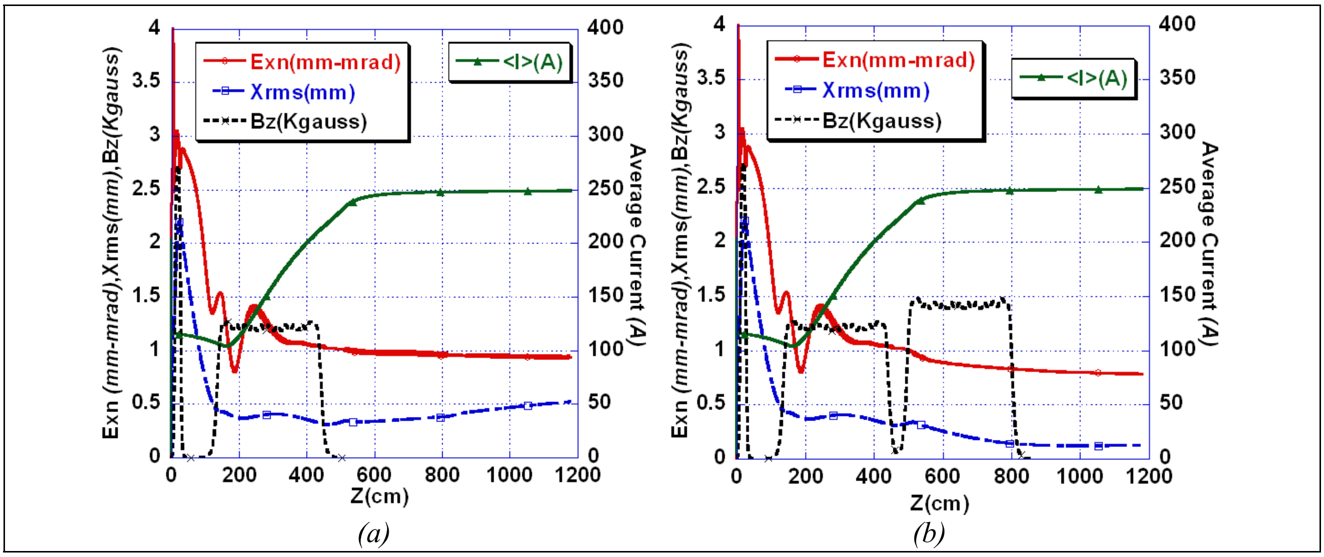


*Fig. 7 Emittance and envelope vs z for a <I>=249 A beam: (a) only solenoid #1 on (b) solenoids #1 and #2*

### *2.1.3 High compression region (up to 458 A-139 MeV)*

In this region, corresponding to a range of RF compressor phase between -83° and -87°, the phase spectrum presents a high distorsion passing from a triangular shape to a high spike with a long tail (fig.8). The sensitivity to phase jitter reaches a maximum value of $\Delta I/\Delta\varphi$~80A/deg.
An interesting working point (fig.9) in this region, also in view of a further magnetic compression, is represented by the point with $\varphi_{RF\ comp}$= -85° corresponding to a current of 320 A. The projected emittance is ~ 1 mm mrad and the distorsion of the longitudinal phase space does not yet prevents a further compression.

In figure 10 the results of the slice analysis show that this working point gives a maximum slice current of 581 A with an emittance of ~0.74 mm mrad.

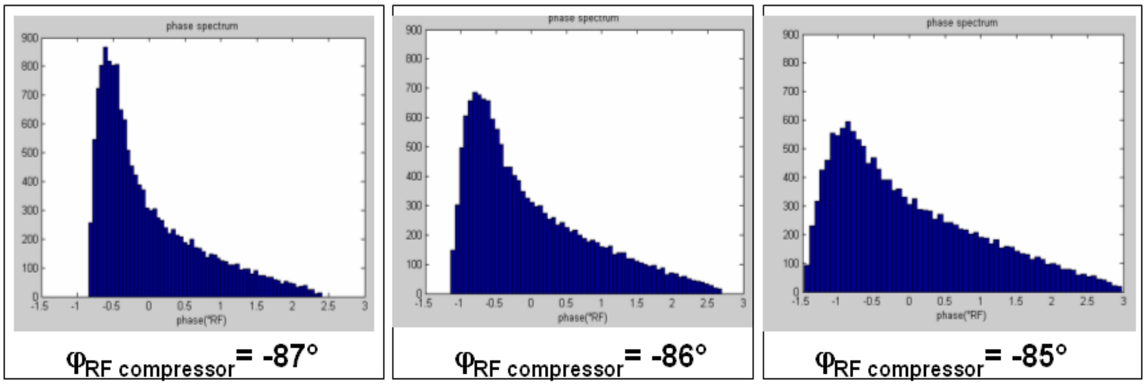


*Fig.8 Evolution of the bunch shape with RF compressor phase in the high compression region*

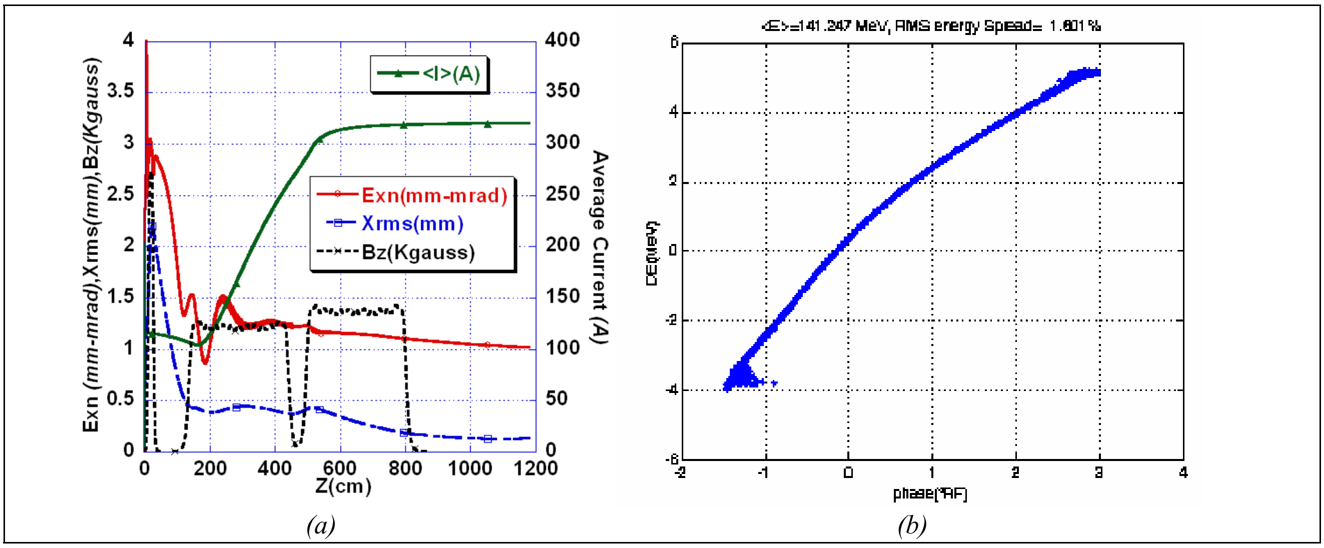


*Fig.9 <I>=320 A beam: (a) Emittance, envelope,current,Bz vs z (b) φ-E space*

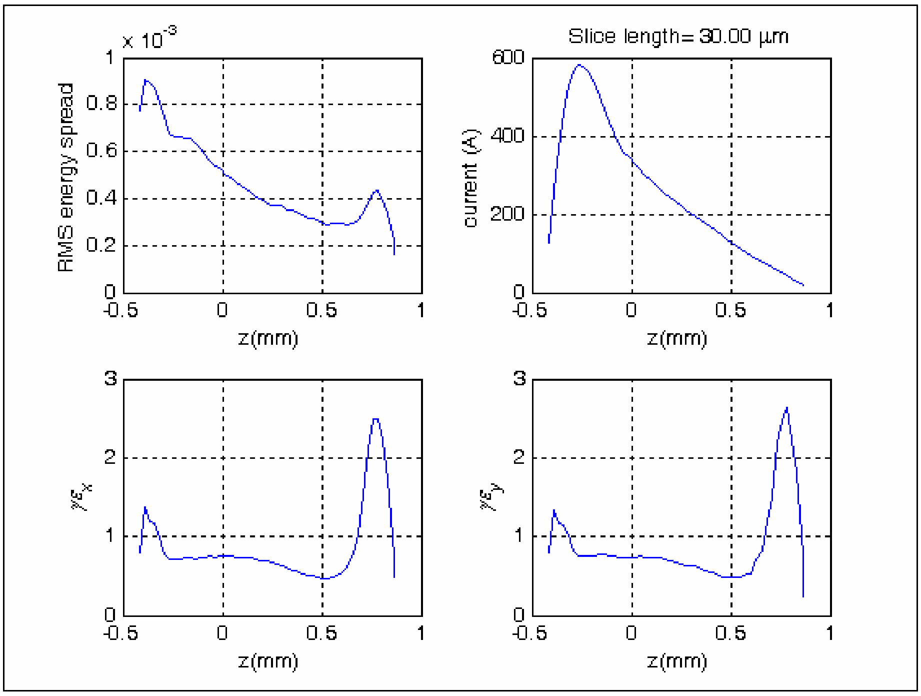


*Fig.10 <I>=320 A beam: slice analysis*

### *2.1.4 Over compression region (up to 1180 A-138 MeV)*

In this region the very high distorsion of the bunch shape (fig.11), the strong sensitivity to phase jitter up to $\Delta I/\Delta\varphi \sim 218$A/deg and the proximity to the possibility of debunching (fig.12) prevent the possibility of an efficient use of the compression.

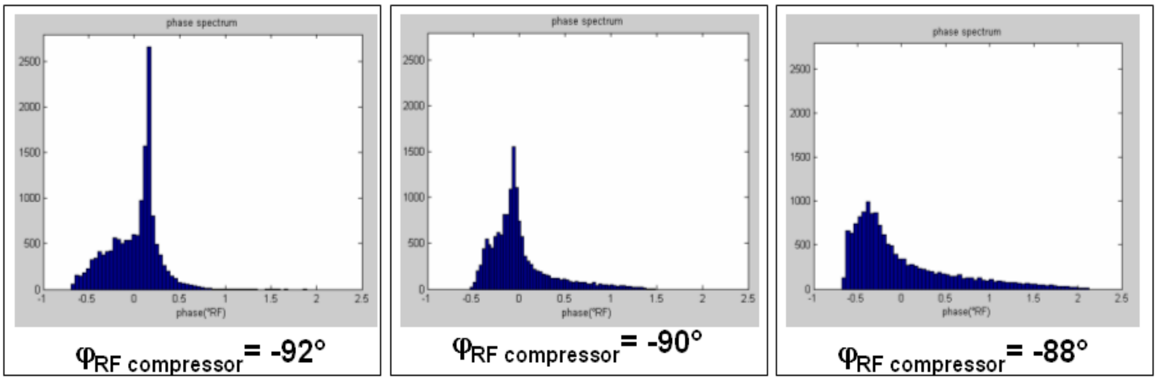


*Fig.11 Evolution of the bunch shape with RF compressor phase in the over compression region*

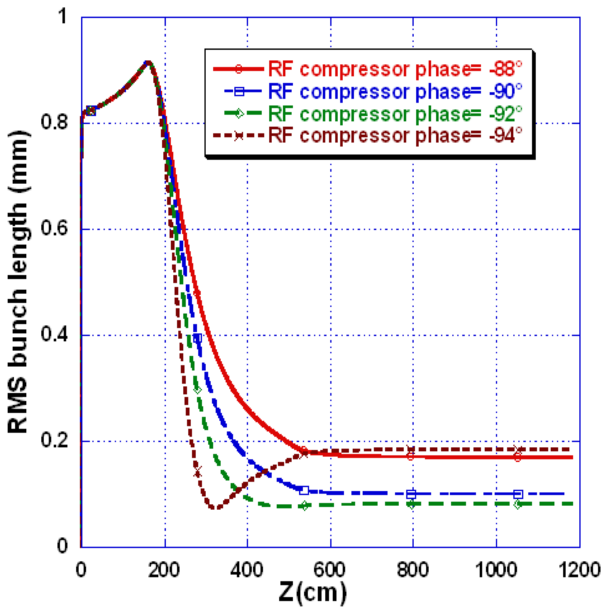


*Fig.12 Evolution of the rms bunch length vs z in the over- compression region*

In addition also the emittance control becomes problematic at these very high levels of compression. In order to contain the emittance growth it is necessary to use the possibility of finel tuning offered by the SPARC solenoids.

In fact each solenoid is composed by an array of 13 coils in which the first coil and the next coils in groups of 3 can be supplied independently (fig.13).

Figures 14 and 15 show the emittance evolution in this compression regime for the two different tunings of the magnetic field specified in table 1: the first one minimizes the final emittance for $\varphi_{RFcomp}=-88°-\langle I\rangle=566$ A and the second one minimizes the final emittance for higher current values (up to the limit value of 1180 A).

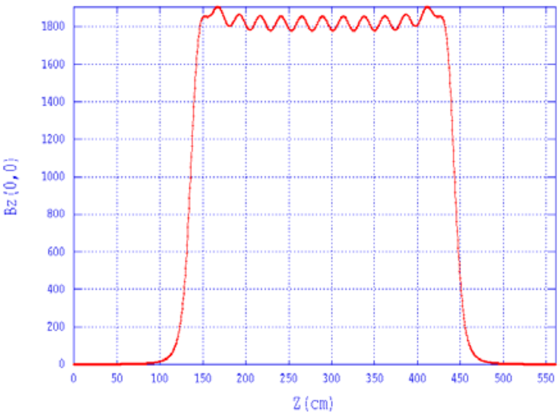


*Fig.13 TW section magnetic field on axis of the SPARC solenoid (13 coils in a closed iron screen) at the max. excitation current*

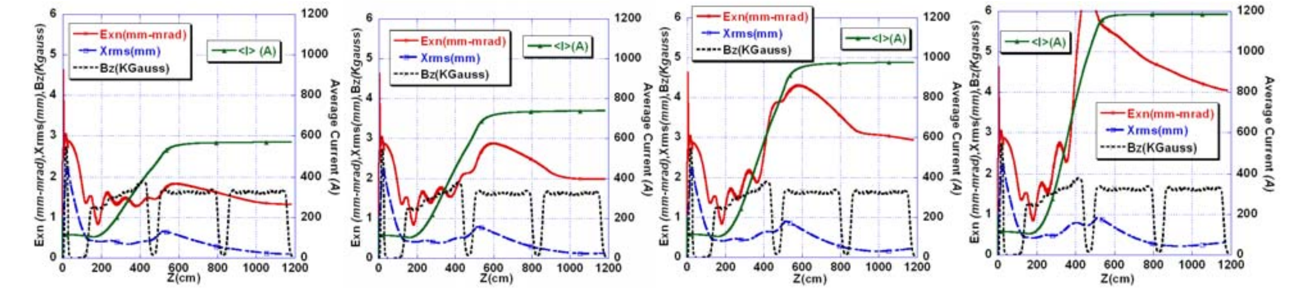


(a) (b) (c)

*Fig.14 Emittance ,current, envelope and magnetic field vs z for setting#1:(a) $\varphi_{RFcomp}$=-88°,<I>=566 A (b) $\varphi_{RFcomp}$=-89°,<I>=732 A (c) $\varphi_{RFcomp}$=-90°,<I>= 962 A(d) $\varphi_{RFcomp}$=-91°,<I>= 1180 A*

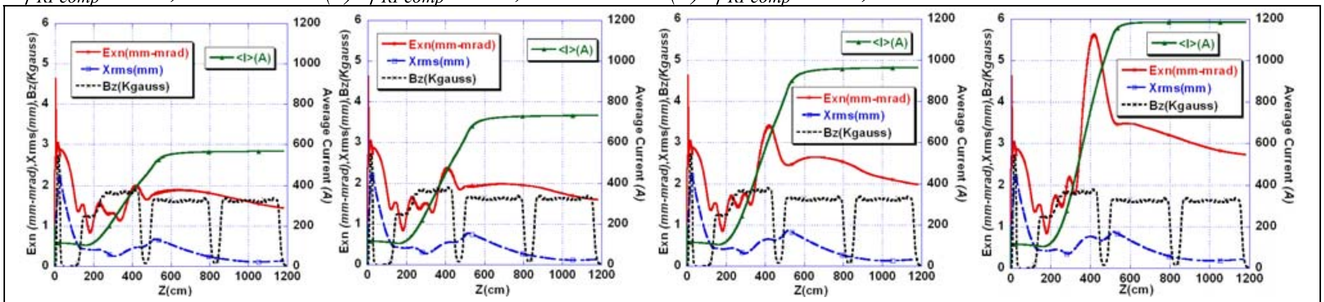


(a) (b) (c) (d)

*Fig.15 Emittance ,current, envelope and magnetic field vs z for setting#2:(a) $\varphi_{RFcomp}$=-88°,<I>=566 A (b) $\varphi_{RFcomp}$=-89°,<I>=732 (c) $\varphi_{RFcomp}$=-90°,<I>= 962 A (d) $\varphi_{RFcomp}$=-91°,<I>= 1180 A*

*Table 1 Two possible settings for the fine tuning of the TW sections magnetic field*

| | **SETTING #1** | **SETTING #2** |
|---|---|---|
| **B1 (gauss):** | | |
| *coil1* | 1200 | 1200 |
| *coil2* | 1200 | 1200 |
| *coil3* | 1200 | 1200 |
| *coil4* | 1200 | 1200 |
| *coil5* | 1500 | 1800 |
| *coil6* | 1500 | 1800 |
| *coil7* | 1500 | 1800 |
| *coil8* | 1600 | 1800 |
| *coil9* | 1600 | 1800 |
| *coil10* | 1600 | 1800 |
| *coil11* | 1800 | 1800 |
| *coil12* | 1800 | 1800 |
| *coil13* | 1800 | 1800 |
| **B2 (gauss)** | 1600 | 1600 |
| **B3 (gauss)** | 1600 | 1600 |

It is interesting to observe what happens during the compression in this very high level compression regime due the strong combined effect of RF and space charge non linearity: as it is shown in figure 16 if we divide the bunch in a fixed number of longitudinal slices, they tend to overlap and this effect increases with the increase of the compression.

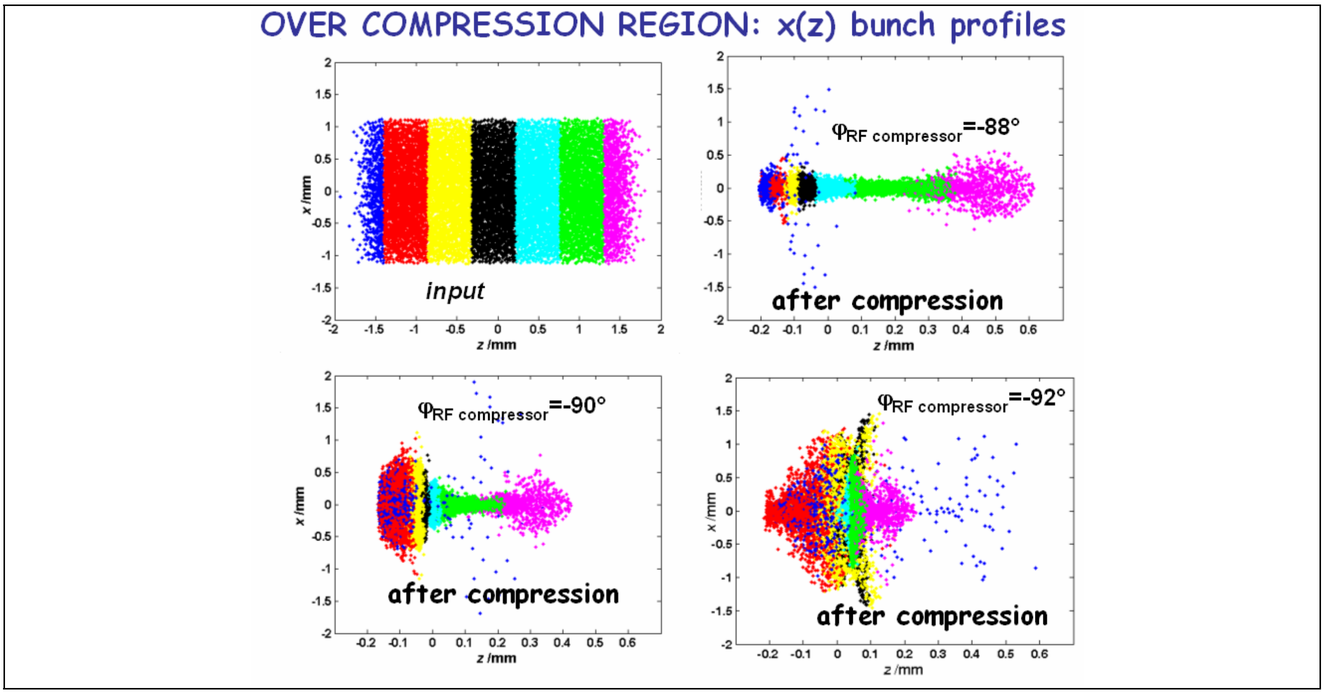


*Fig.16 Slice model for the bunch for different values of the RF compressor phase in the over compression region*

### *2.1.5 Summary of the results*

The results of the numerical investigation reported above, summarized in table 2, demonstrate that also without the use of a 4$^{th}$ harmonic section placed before the RF compressor it is possible to reach good levels of compression with a good control of emittance.
Some useful working points have been identified:

1. <I>=150 A , <E>= 150 MeV, ε=0.7 mm mrad for FEL experiments driven by a chirped high brightness beam in SPARC I
2. <I>=249 A , <E>= 143 MeV, ε=0.8 mm mrad for FEL experiments driven by a chirped high brightness beam in SPARC II
3. <I>=320 A , <E>= 141 MeV, ε=1 mm mrad coupled to a magnetic compressor in the *SPARXINO* test facility [3]

However for higher levels of compression some undesired characteristics limit the practical use of high levels of RF compression especially in view of a further compression at higher energy.

*Table 2: RF compressor parameters*

| RF compressor phase range | B1,B2,B3 (gauss) | Current (A) | Max. Emittance (μm) |
|---|---|---|---|
| -60° / -75° | 1200,0,0 | 117-151 | 0.7 |
| -75° / -83° | 1200,1400,0 | 151-249 | 0.8 |
| -83° / -87° | 1200,1400,0 | 249-458 | 1.25 |
| -87° / -91° | Ramped from 1200 to 1800,1600,1600 | 458-1180 | 2.8 |

In fact the increase of compression gives: 1) an increasing deformation in the shape of the bunch that appears as a spike followed by a long tail 2) a highly non linear longitudinal phase space 3) a strong sensitivity to phase jitter that gives, for compression factors greater than 3, a percentage variation of current of ~ 15-25% for an error phase of 1 deg on the RF compressor.
These effects are due to the combination of the RF and space charge non-linearities. A partial compensation can be obtained by the foreseen IV harmonic section placed between the gun and the RF compressor.

## *2.2 IV harmonic section included*

### *2.2.1 The principle of operation*

With the 11424 MHz section switched on, the optimization criterion is to bunch the beam in the centre with a linear correlation phase-energy differently from the unlinearized case where the charge piles up in the bunch head and only a portion of the electrons (typically the half) is involved by the compression process.
The use of a higher harmonic cavity in order to linearize the longitudinal phase space is based on the following simple analytical considerations:
due to the sinusoidal nature of RF voltage

$$V = V_0 \sin(\phi_0) + \Delta\phi V_0 \cos(\phi_0) - \frac{1}{2}\Delta\phi^2 V_0 \sin(\phi_0) + \ldots$$

The second order term in V can be cancelled by using a higher harmonic cavity

$$V_h = V_h \sin(\phi_h) + h\Delta\phi V_h \cos(\phi_h) - \frac{1}{2}(h\Delta\phi)^2 V_h \sin(\phi_h) + \ldots$$

with a decelerating phase $\varphi_h$.
Working on crest ($\sin\varphi_0=1$) the compensation occours for $V_h=V_0/h^2$ and $\sin\varphi_h = -1$: in our case $h$=4 and the maximum value of $V_h$ is 4.7 MeV.
In presence of compression this value is reduced because the energy gain in the RF compressor is lower.
In addition due to the deceleration the input energy and energy spread change give different energy gain and phase slippage in the SLAC sections, so that the amount of the needed deceleration must be determined numerically.
The mechanism of linearization realized in this way in absence of space charge is illustrated in figs 17 and 18 showing the longitudinal phase space and the phase and energy distributions in the bunch with and without the IV harmonic section: one can see that the RF curvature of the longitudinal phase space gives a peak in the phase spectrum that can be corrected by a proper shaping of the longitudinal phase space at the entrance of the first TW linac.
In this way it is possible to obtain a perfect linearization of the φ-E space and a uniform distribution in the bunch.

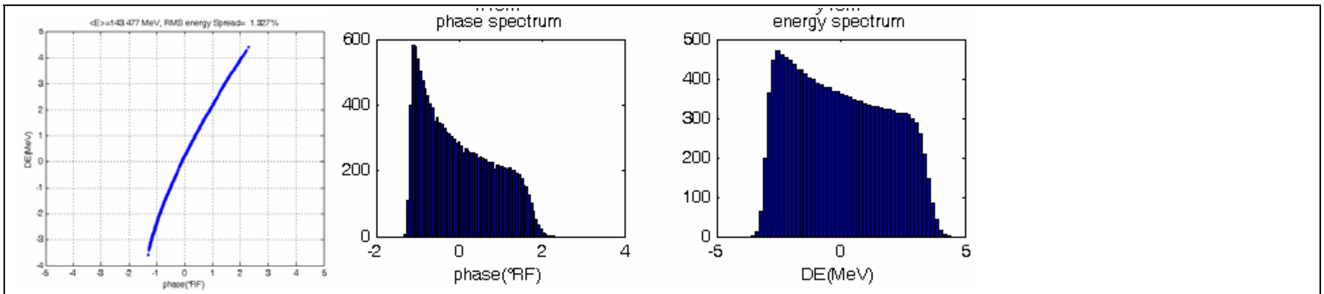


*(a)* *(b)*

*Fig.17 IV harmonic cavity off and space charge off at TW linac output: (a)φ-E space (b) phase and energy spectrum*

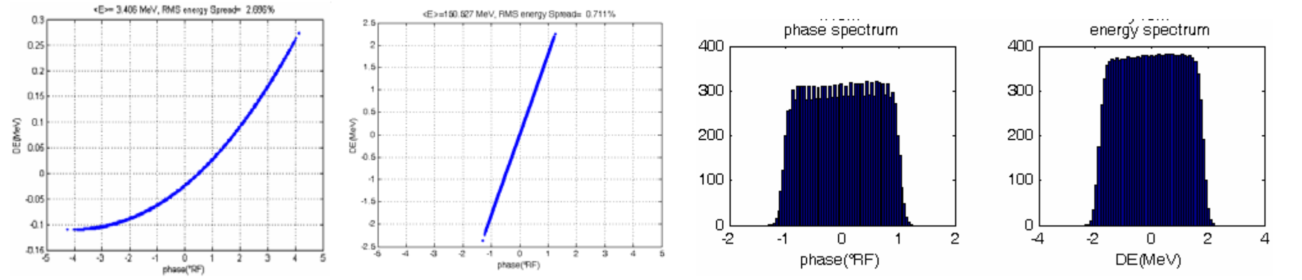


*(a)* *(b)* *(c)*

*Fig.18 IV harmonic cavity on and space charge off: (a) φ-E space at TW linac input (b) φ-E space at TW linac output (b) phase and energy spectrum at TW linac output*

As we will see in the following, this linearization process is complicated by the presence of space charge that prevents to obtain a complete linear longitudinal phase space..

### *2.2.2 Parameters optimization*

From PARMELA simulations it results that, in order to satisfy the optimization criterion described above, the beam energy must be reduced from 5.64 MeV to ~3.3 MeV, that can be obtained by different combinations of phase ($\varphi_X$) and amplitude ($E_X$) in the X-band section (fig. 19a), giving different compression factors for the same phase on the RF compressor.
As it is shown in figure 19b the beam current can be raised to ~ 950 A.

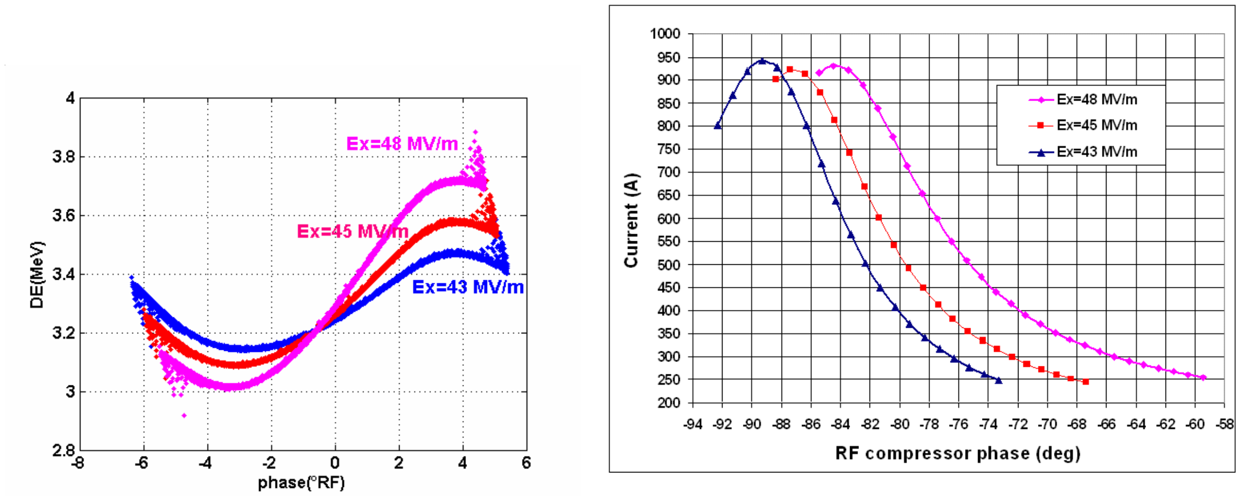


*(a)* *(b)*

*Fig.19 (a) Longitudinal phase space at the first accelerating section entrance (b) Final current vs RF compressor phase for different electric fields amplitude in the X. band section and the same decelerating voltage*

In the range 300-900 A the curves of fig.19b have been fitted by a 4$^{th}$ order polynomial whose derivative gives the sensitivity to the RF compressor phase jitter: in figure 20 the quantity $(dI/d\varphi)/I$ is plotted vs the beam current for these three curves compared with the case of compression without IV harmonic section. The sensitivity to phase jitter is reduced of a factor ≥2 by the use of the IV harmonic section.

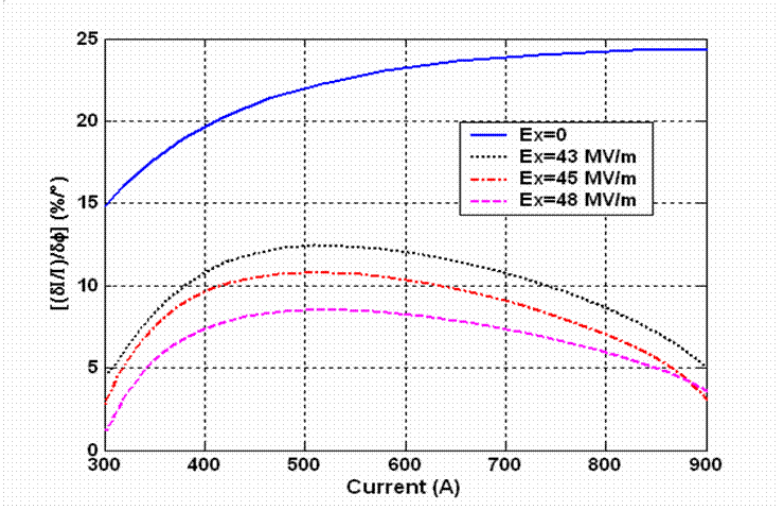


*Fig.20 The percentage variation of current for an error of 1 degree in the RF compressor phase*

### ***2.2.3 Working points in medium and high compression regime***

In the parameters space of figure 19 two working points have been selected also in view of the application of the system as injector of the so-called *SPARXINO* 3-5 nm FEL test facility [3] based on an upgrade of the actual Frascati 800 MeV linac including a second stage of compression of magnetic type.

The first working point (fig.21a,b,c) obtained by using Ex=43 MV/m and $\varphi_{RFcomp}$= -81° is particularly suitable to a further magnetic compression due to its good beam characteristics in terms of current (450 A) and emittance (1.03 μm) and good linearity of φ-E space compared with the case in which the same bunch length is obtained without the use of the IV harmonic section.

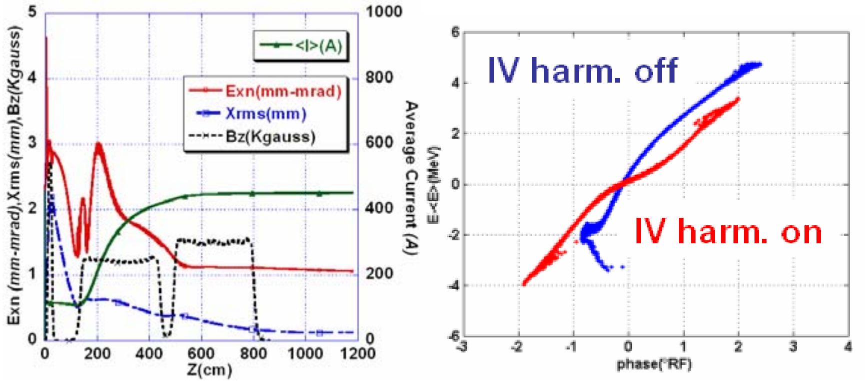


*(a)* *(b)*

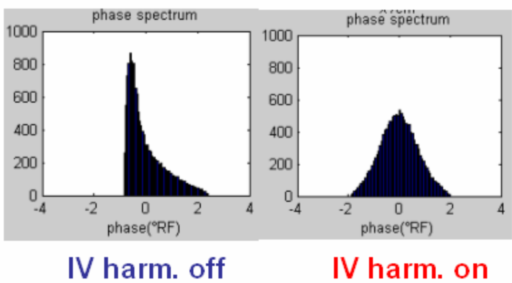


*(c)*

*Fig.21 <I>=450 A compressed beam: (a) Transverse emittance, current,envelope and axial magnetic field distribution vs z (b) Longitudinal phase space for a 450 A compressed beam obtained with and without the IV harmonic section (c)phase spectrum for a 450 A compressed beam obtained with and without the IV harmonic section*

The relative slice analysis for a slice length of 30 μm shown in figure 22 indicates that the compression occours in the central part of the bunch, where the energy spread and emittance are at a minimum, that maximizes the normalized brightness, $B_n=I/(4\pi\varepsilon_{nx}\varepsilon_{ny})$, that reaches $6\cdot10^{13}$ for the central slice.

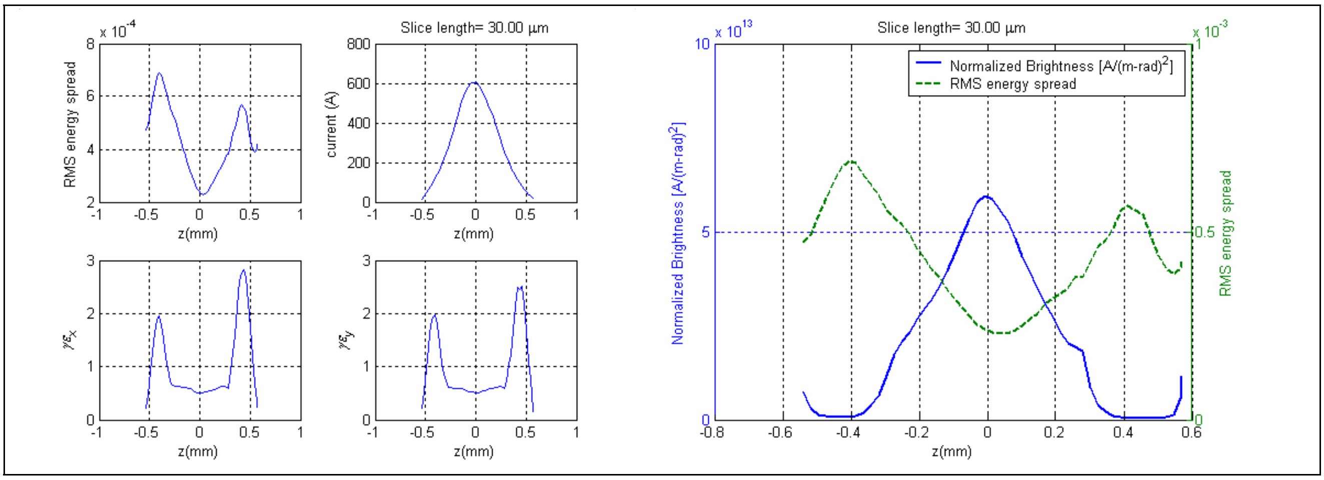


*Fig.22 Slice analysis for a 450 A compressed beam*

The second working point (figs. 23 and 24) obtained by using Ex=45 MV/m and $\varphi_{RFcomp}$= -84° is interesting for its high current (860 A) and very good control of the projected (1.5 μm) and slice emittance allowing to rise the peak brightness to $1.13\cdot10^{14}$.

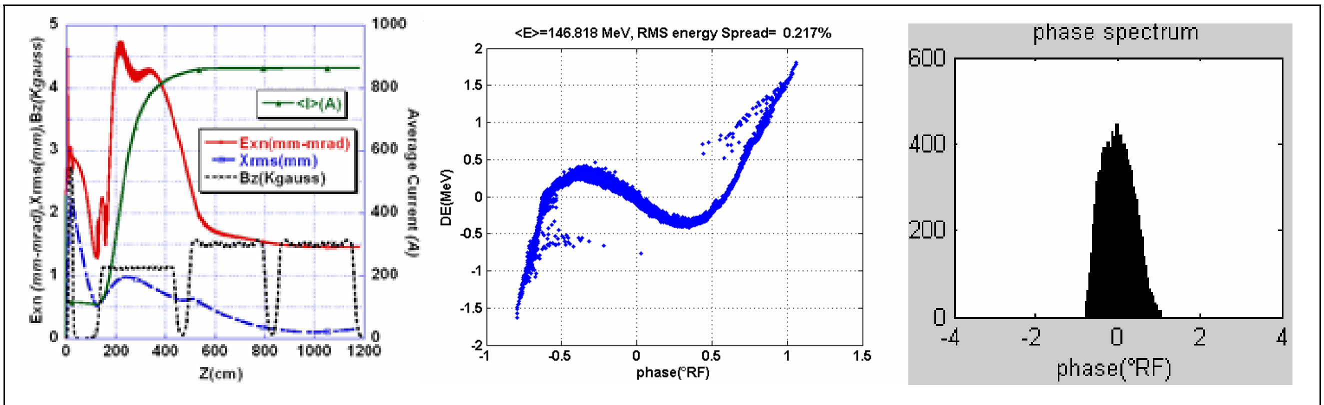


(a) (b) (c)

*Fig.23<I>=860 A compressed beam (a) Transverse emittance, current, envelope and axial magnetic field distribution vs z (b) φ-E space (c) phase spectrum*

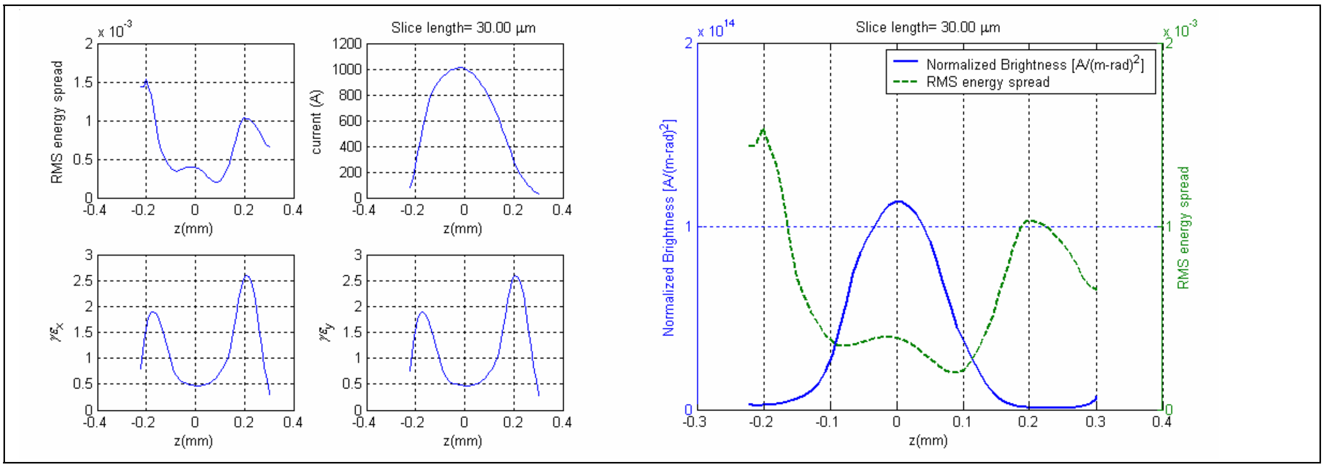


*Fig.24 Slice analysis for a 860 A compressed beam*

Intermediate values of current (500-700 A) can be obtained also with good properties in terms of projected and slice emittance and can be usefully tested in SPARC phase II, but the space charge prevents to get a complete linear longitudinal phase space that results less suitable to a further magnetic compression being the slope of the curve φ-E reduced in the bunch centre respect to the tails.
In fact, as it is put in evidence in fig.25, showing the longitudinal phase space for different values of the RF compressor phase, the space charge tends to reduce the energy spread in the centre of the bunch where the compression occours, preventing a complete 90° rotation (as it should be foreseen by the velocity bunching theory in absence of space charge [4]).
Of course this is a good feature from the point of view of the bunch because allows contemporary to maximize peak current and minimize energy spread, but is a problem for a next compression stage that requires a φ-E correlation in the bunch.

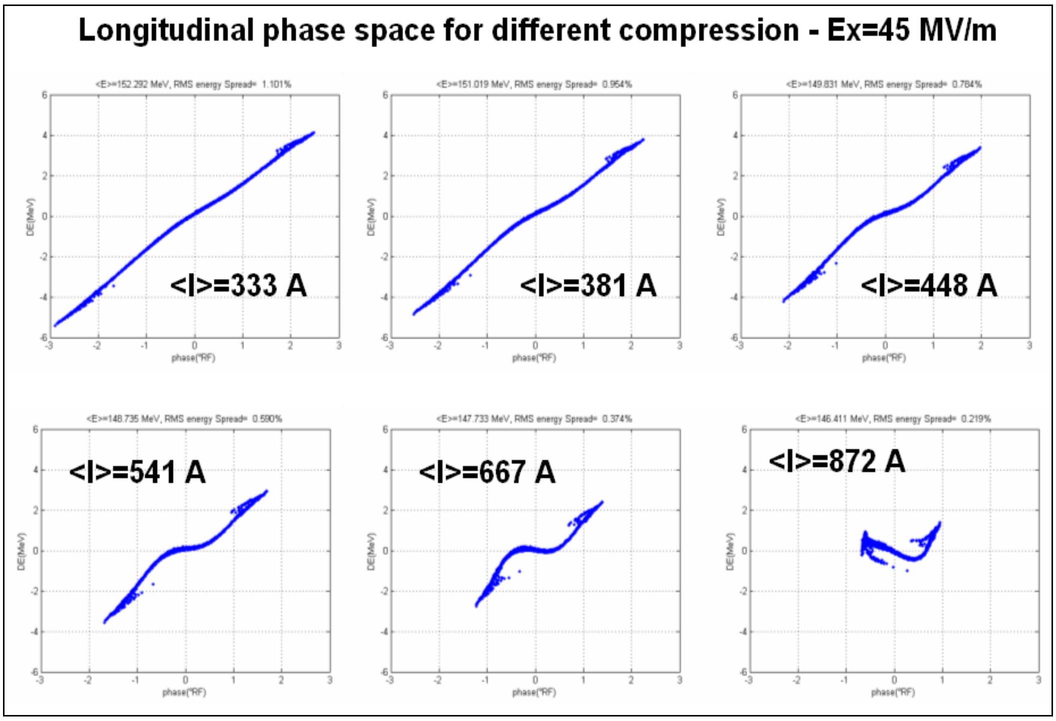


*Fig.25 Longitudinal phase space for different compressions*

## 3 STABILITY ANALYSIS

A systematic scan of the main parameters affecting the compression for three different values of current (338A, 450A, 860 A) was done around the reference value in order to derive the tolerance on each parameter.
The parameters that have been taken into account in this analysis are:

- phase and electric field amplitude on X section
- phase of RF compressor linac
- magnetic field strength on TW sections

It was adopted the criterion of keeping the percentage variation of current and the emittance growth below respectively below 15% and 10% as it is shown in the plots of fig. 26.

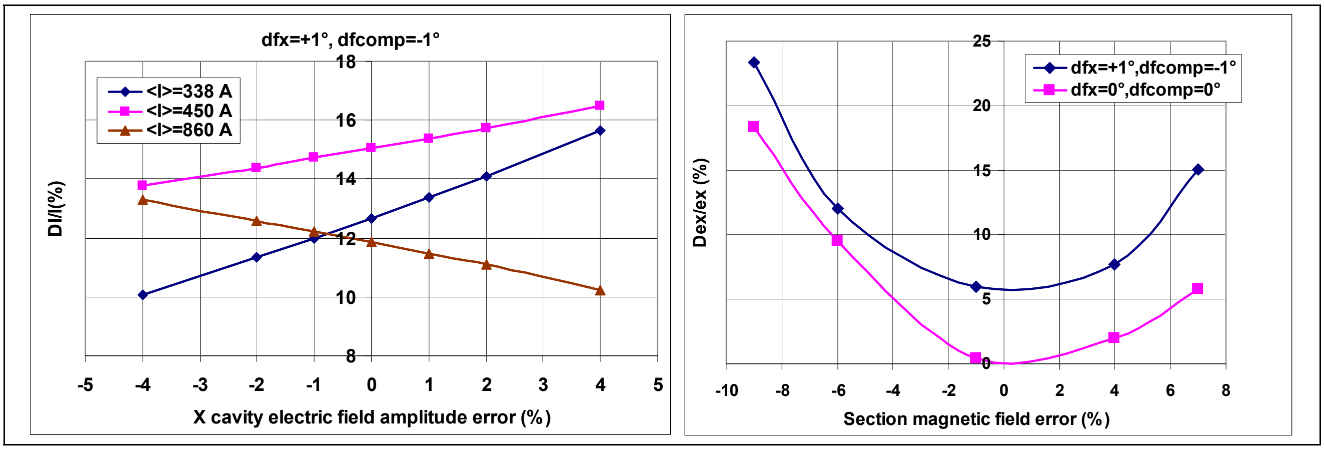


*Fig.26 Results of systematic scan of the main parameters affecting the compression*

This procedure gave the tolerances on the different tuning parameters listed in table 2.

Table 2 Tolerances relative to the main parameters affecting the compression

| | |
|---|---|
| RF compressor phase $\delta\varphi_{RFcomp}$ | ± 1° |
| X cavity $\delta\varphi_X$ | ± 1° |
| X cavity electric field amplitude δEx/Ex | ± 0.5% |
| TW section magnetic field | ± 5 % |

## 4 STATISTICAL STUDY OF SENSITIVITY TO COMBINED ERRORS

The global stability of the two working points described in the paragraph 2.2.3 (450A and 860 A) and their sensitivity to various types of random errors, under realistic conditions has also been studied. Following a technique already used for the stability study of the 100 A non compressed beam in the SPARC nominal working point described in [9], a statistical analysis has been done based on the results of one hundred PARMELA runs performed for each working point, each one with random error sets within the limits reported in table 3 set using the criterion of having a maximum increase of the projected emittance of 10% with respect to the nominal case. One hundred simulations runs were done each with errors set randomly according with the "latin hypercube" sampling technique assuring that the numbers used are uniform distributions within the error limits listed in table 3.

*Table 3: Variation of parameters for combined random errors study*

| **Parameter** | **Error range** |
|---|---|
| Phase jitter gun-linac | ±1° |
| Phase jitter gun-X band section | ±1° |
| Charge fluctuation | 10% |
| Gun B field amplitude | ±0.4% |
| Gun E field amplitude | ±0.5% |
| Spot radius | ±10% |
| Spot ellipticity | 3.5% |

The results of the simulations were used to construct the curves plotted in fig. 27 that give the probability to obtain an emittance greater or equal than the corresponding value on the abscissa for the two considered compressed beams compared with the non-compressed SPARC beam. One can observe for example that a probability of 10% corresponds to a normalized projected emittance ≥ 1 μm for the SPARC working point and to about 1.8 μm at 450 A and to about 2.25 μm at 860 A..

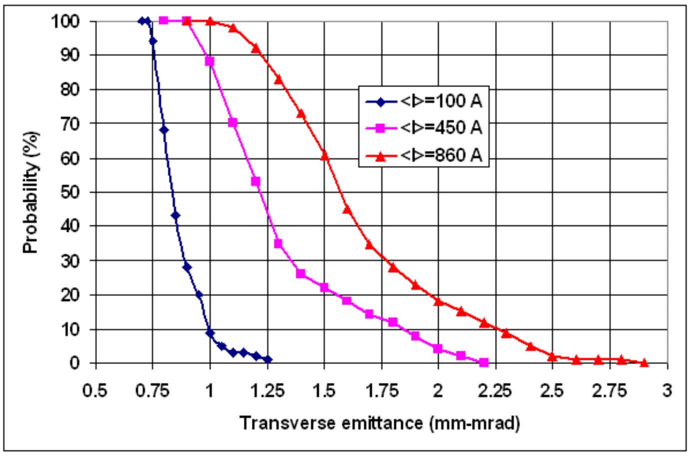


*Figure 27: Probability vs emittance over 100 simulations*

The distribution of the values of the projected normalized brightness in 100 runs gives the results reported in figure 28 showing that the compression increases, as expected, not only the average value but also the standard deviation with a consequent reduction of the brightness stability.

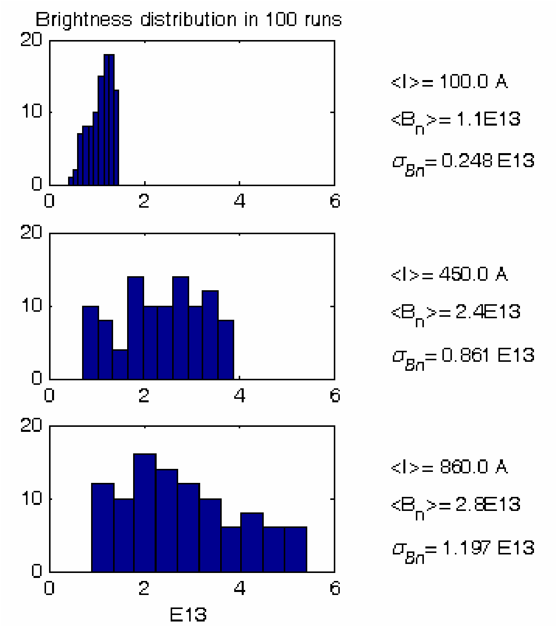


*Fig. 28 Brightness distribution over 100 simulations*

Concerning the slice emittance, in the 100 simulations it does not exceed 1 μm for the central slices at 450 A and 1.2 μm at 860 A.

## 5 CONCLUSIONS

The results of the RF compressor optimization study in the SPARC-phase II layout showed that a high peak current beam (up to 1 KA in the slice) can be produced with a charge uniformly distributed through the pulse and a tolerable sensitivity on incoming phase jitter, also if the space charge prevents to get a complete linear longitudinal phase space.

A sensitivity study to various types of random errors in some significant operating points showed that the projected and slice emittance remain respectively below 2.5 μm and 1.2 μm in realistic operation conditions.

## REFERENCES

[1] SPARC collaboration "Status of the SPARC Project", presented to PAC05 Conference
[2] A. Bacci et al., SPARC-RF-03 / 001
[3] M. Boscolo et al. "Start To End Simulations for The SPARX Project", presented to PAC05 Conference
[4] L. Serafini, A. Bacci, M. Ferrario , "Ultra-short electron bunch generation with a rectilinear compressor," Proceedings of PAC2001, Chicago, June 2001.
[5] M. Ferrario et al. " Beam dynamics study of an RF bunch compressor for High Brightness beam injectors", Proceedings of EPAC02, p. 1762, June 2002 Paris
[6] P. Piot et al. "Subpicosecond compression by velocity bunching in a photoinjector", ", Phys. Rev. ST Accel. Beams 6, 033503 (2003)
[7] S.G. Anderson et al. "Velocity bunching of high brightness electron beams", Phys. Rev. ST Accel. Beams 8, 014401 (2005)
[8] J. Billen, "PARMELA", LA-UR-96-1835, 1996
[9] M. Biagini et al. "SPARC photoinjector working point optimization, tolerances and sensitivity to errors", Proceedings of EPAC04, p.396, July 2004 Lucerne